

ENVIRONMENTAL RESEARCH
LETTERS

LETTER

OPEN ACCESS

RECEIVED
25 March 2022REVISED
17 August 2022ACCEPTED FOR PUBLICATION
24 August 2022PUBLISHED
7 September 2022

Original content from
this work may be used
under the terms of the
[Creative Commons
Attribution 4.0 licence](#).

Any further distribution
of this work must
maintain attribution to
the author(s) and the title
of the work, journal
citation and DOI.

Reversed and comparable climate impacts from historical
anthropogenic aerosol and GHG on global-scale tropical cyclone
genesis potentialJian Cao^{1,2,*} , Hao Wang¹, Haikun Zhao^{1,*} , Bin Wang^{2,3}, Liguang Wu⁴ and Chao Wang^{1,2}

¹ Key Laboratory of Meteorological Disaster, Ministry of Education/Joint International Research Laboratory of Climate and Environment Change/Collaborative Innovation Center on Forecast and Evaluation of Meteorological Disasters, Nanjing University of Information Science and Technology, Nanjing, People's Republic of China

² Earth System Modeling Center, Nanjing University of Information Science and Technology, Nanjing, People's Republic of China

³ Department of Atmospheric Sciences, University of Hawaii at Mānoa, Honolulu, HI, United States of America

⁴ Department of Atmospheric and Oceanic Sciences and Institute of Atmospheric Sciences, Fudan University, Shanghai, People's Republic of China

* Authors to whom any correspondence should be addressed.

E-mail: JianC@nuist.edu.cn and zhk2004y@gmail.com

Keywords: anthropogenic forcing, tropical cyclone, genesis potential index, aerosol, GHG

Supplementary material for this article is available [online](#)

Abstract

Emissions of anthropogenic aerosol and greenhouse gases (GHG) have significantly altered various aspects of the climate extremes in recent decades, yet, the observed global tropical cyclone frequency (TCF) shows no significant trend. Untangling this puzzle requires a better understanding of the precise contributions of the individual anthropogenic forcing to global TCF changes. Here, we quantify the relative contributions of anthropogenic aerosol and GHG to global TCF, represented by genesis potential index (GPI), using the single anthropogenic forcing experiments from the 14 Coupled Model Intercomparison Project phase 6 (CMIP6) models. We find that the two forcings have comparable but opposite impacts on GPIs due to their influences on the TC environment, leading to an insignificant change in GPIs in the historical period (1850–2014). Notably, the aerosol radiative forcing's intensity is only about one-third of that of GHG, suggesting a more effective modulation of aerosol forcing on GPIs. The stable global TC frequency during the past decades could be attributable to the similar pace of the two anthropogenic emissions. The results highlight that a reliable global TC projection depends on both the aerosol and GHG emission policies.

1. Introduction

Extensive studies have documented the significant impacts of anthropogenic forcing on global TC activities regarding its nontrivial social-economic impact and great scientific merit (Webster *et al* 2005, Murakami *et al* 2020, Knutson *et al* 2019). The anthropogenic forcing-induced global warming is significant during the historical period and projects to be further amplified, thus probably changing TC activities (Webster *et al* 2005, Knutson *et al* 2010, 2020, Walsh *et al* 2016). Nevertheless, the observed global TCF shows no long-term trend during the past decades (Webster *et al* 2005, Knutson *et al* 2019), yet no consensus has been made regarding how

global TCF will change in a future warming climate (Camargo *et al* 2013, Knutson *et al* 2020, Emanuel 2021). Most studies implicitly hypothesized the similar impacts of different forcing agents on global TCF for different emission scenarios, yielding the controversial results of TCF projection (Camargo *et al* 2013, Sugi and Yoshimura 2012, Bhatia *et al* 2018, Lee *et al* 2020, Emanuel 2021).

However, studies showed that the TCF may be sensitive to forcing types since their impacts on TC-related environments vary. The greenhouse gas (GHG) forcing-induced top-heavy warming could suppress the upward mass flux, thus reducing the global TCF, with large zonal variations (Sugi and Yoshimura 2012, Satoh *et al* 2015). The increase of

troposphere aerosol from intensive volcanic eruptions or artificial injection could shift the TC genesis location meridionally within one hemisphere (Jones *et al* 2017, Wang *et al* 2018, Pausata and Camargo 2019). Recently, Cao *et al* (2021) pointed out that the historical anthropogenic aerosol loading could shape the hemisphere-asymmetric response of TCF through an aerosol-forced significant change of meridional gradient of surface temperature. It promotes Southern Hemisphere (SH) TCs by weakening vertical wind shear (VWS) and strengthening vertical motion but reduces the Northern Hemisphere (NH) TCs from enhanced VWS and reduced vertical motion. In summary, these studies indicated changes in hemisphere-scale and global-scale TCF are potentially sensitive to different forcing agents.

TC forms over the tropical oceans, its formation is determined mainly by its ambient large-scale environment. The frequency of TC could be theoretically and empirically expressed by the TC ambient environmental conditions, including the maximum potential intensity (PI), VWS, relative humidity (RH), and vertical velocity (Ω) (e.g. Emanuel and Nolan 2004, Wang and Murakami 2020). Anthropogenic aerosols and GHG are the two leading components of external forcings during the historical period, which showed a similar spatial pattern of climate impacts over the tropics, albeit its different signs (Xie *et al* 2013, Persad *et al* 2018). The opposite impacts from the two forcings may be implicit in the canceling effect on the TC-related environment. Indeed, Ting *et al* (2015) found that the decrease in TC maximum PI due to aerosol forcing could essentially cancel out the increase of PI from the GHG forcing. Such comparable and opposite impacts of aerosol and GHG forcing on PI are still held over global and hemisphere scales (Sobel *et al* 2016). In addition, observational studies suggested that the total effect of the two forcings on observed global TC activities is relatively small during the historical period (Knutson *et al* 2019), which may be due to their opposite climate impacts on TCs (Weinkle *et al* 2012, Villarini and Vecchi 2013, Ting *et al* 2015, Sobel *et al* 2016, 2019, Knutson *et al* 2019).

However, to date, it is still unknown whether this cancelation effect is also existing for TCF or not, and what is the relative importance of historical aerosol and GHG forcing on global/regional TCF changes. The limitation of its physical mechanism understanding is the main obstacle to uncovering the inconspicuous change of observed global TCF and improving the TCF projection, since the temporal evolutions of aerosol and GHG forcing are different among scenarios in the phases of CMIP (Taylor *et al* 2012, O'Neill *et al* 2016). Motivated by these above studies, questions naturally arose: Do the comparable and opposite impacts of the two forcings on global TCF exist? Is the global TCF more sensitive to aerosol forcing than

GHG forcing, since the smaller radiative forcing from anthropogenic aerosol during the historical period? Here, we intended to explore the climate effect of historical aerosol and GHG forcing on global TCF and quantify the relative importance of the two forcings on TCF changes based on the single forcing simulations of the CMIP6 models.

2. Data and method

2.1. Simulations and data

To identify how individual anthropogenic forcing affects global TCs, we selected the monthly outputs of four experiments, historical, historical aerosol-only (hist-aer), historical GHG-only (hist-GHG), and pre-industrial simulations, from 14 CMIP6 models (table 1). The historical experiment is forced by the time-varying all-known historical (ALL) forcing, while the hist-aer and hist-GHG simulation only considered the time-varying historical anthropogenic aerosol and GHG forcing with the other forcing fixed at the pre-industrial level, respectively (Eyring *et al* 2016, Gillett *et al* 2016). The pre-industrial simulation is forced by the perpetual 1850s forcings. The last 100 yr data of pre-industrial simulation is used as the reference. The last 30 yr (1985–2014) data from historical, hist-aer, and hist-GHG simulations are used to identify the climate effects of external forcing. Thus, the differences between the periods of 1985–2014 from each forced experiment and the corresponding pre-industrial simulation are regarded as the influences of external forcing. To obtain the multi-model ensemble, we interpreted the model outputs into the resolution of $2^\circ \times 2^\circ$ using bilinear interpolation. The NH TC peak season July–October (JASO) and the SH TC peak season January–April (JFMA) are considered in this study.

In the selected 14 CMIP6 models, 12 models performed the tier-1 experiment of radiative forcing model intercomparison project (RFMIP). The piClim-control, piClim-aer, and piClim-ghg experiments are used to calculate the effective radiative forcing of the historical aerosol and GHG forcing. All experiments are integrated with atmospheric general circulation model forced by climatological sea surface temperature (SST) and sea ice concentration from its corresponding piControl experiment. The external forcing of piClim-control is the same as the pre-industrial simulation. The experimental designs of piClim-aer and piClim-ghg are similar to piClim-control, except using the present-day aerosol and GHG forcing, respectively. The effective radiative forcing of the aerosol (GHG) is defined as the difference of energy budget at the top-of-atmosphere between the piClim-aer (piClim-ghg) and its corresponding piClim-control experiment. Table 1 shows that the ensemble mean of historical aerosol radiative forcing is -1.14 W m^{-2} . It is much smaller than

Table 1. Description of 14 CMIP6 models and the corresponding radiative forcing used in this study.

Model name	Atmosphere resolution Lon × Lat	TOA radiative forcing from aerosols (W m^{-2})	TOA radiative forcing from GHG (W m^{-2})
ACCESS-CM2	192×144	−1.17	3.04
ACCESS-ESM1-5	192×144	−1.25	3.06
BCC-CSM2-MR	320×160	—	—
CESM2	288×192	−1.5	3.03
CanESM5	128×64	−1.11	2.87
CNRM-CM6-1	256×128	−1.14	2.74
FGOALS-g3	180×80	—	—
GFDL-ESM4	288×180	−0.9	3.23
GISS-E2-1-G	90×144	−1.36	2.89
HadGEM3-GC31-LL	192×144	−1.17	3.11
IPSL-CM6A-LR	144×143	−0.68	2.82
MIROC6	256×128	−0.99	2.69
MRI-ESM2-0	320×160	−1.22	3.03
NorESM2-LM	144×96	−1.23	2.8
MME		−1.14	2.94
Standard deviation		0.21	0.16

the radiative forcing from GHG forcing, with a value of $+2.94 \text{ W m}^{-2}$.

2.2. TC genesis potential in climate models

The averaged horizontal resolution of the 14 models is about 200 km over the tropical region. The coarse resolution of these models may limit the ability to simulate TCs. The genesis potential index (GPI) is generally used as a good proxy to represent TCs in coarse resolution models. Two independently developed GPIs by Emanuel and Nolan (2004) and Wang and Murakami (2020) have well representation of TCF climatology and will be adopted in this study. The Emanuel and Nolan's GPI (ENGPI) considers both thermal dynamic and dynamic factors; it is formulated as:

$$ENGPI = |10^5 \eta|^{\frac{3}{2}} \left(\frac{H}{50} \right)^3 \left(\frac{PI}{70} \right)^3 (1 + 0.1 V_{shear})^{-2} \quad (1)$$

where η is the 850 hPa absolute vorticity (Vort), H is the 600 hPa relative humidity, PI is the maximum potential intensity, V_{shear} is the magnitude of 200–850 hPa wind shear. The PI is defined in the following expression:

$$PI^2 = \frac{T_s - T_o}{T_o} \frac{C_k}{C_D} (k^* - k_{RMW}) \quad (2)$$

where $T_s - T_o$ is the temperature difference between the TC outflow (T_o) and SST (T_s); C_k and C_D are bulk exchange coefficients for heat and momentum; and k^* and k_{RMW} are the saturation moist enthalpy of the sea surface and the actual enthalpy of near-surface air in the tropical cyclone eyewall, respectively.

The dynamic GPI (DGPI) from Wang and Murakami (2020) primarily considers the dynamic factors, consists of four elements:

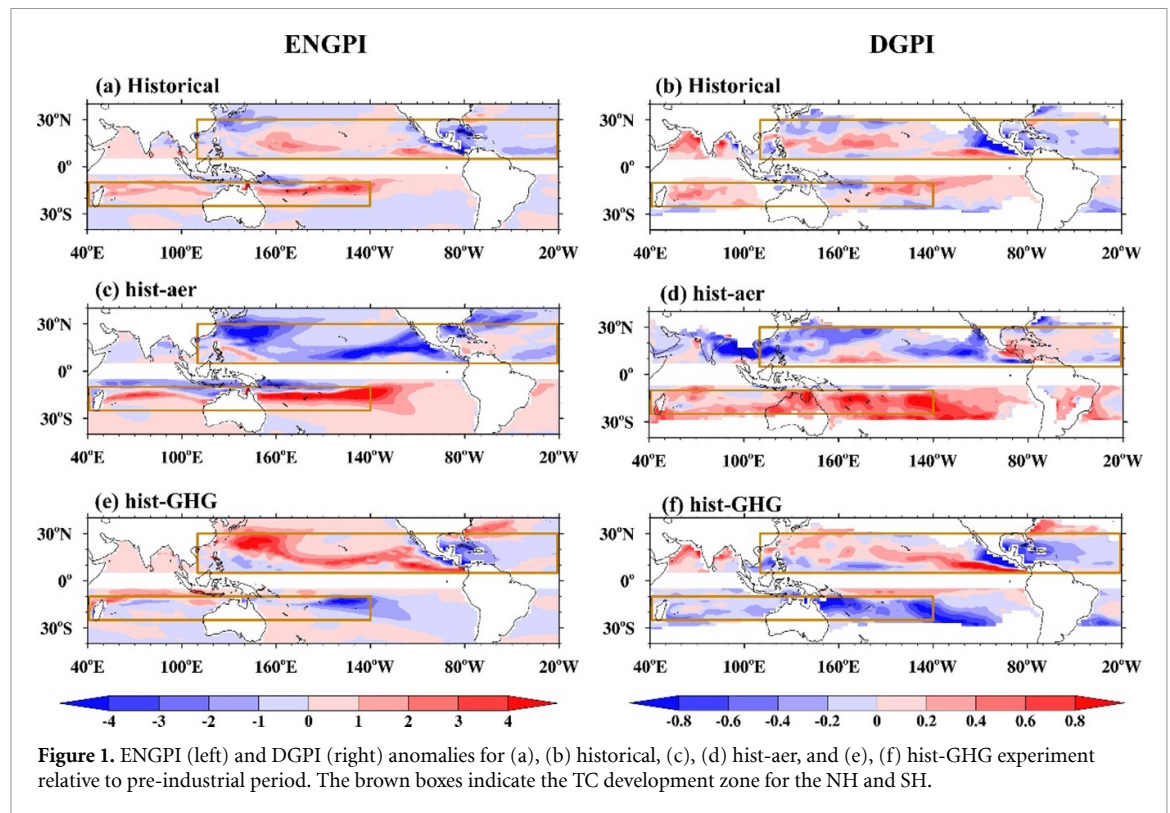
$$DGPI = (2 + 0.1 V_{shear})^{-1.7} \left(5.5 - \frac{\partial u}{\partial x} 10^5 \right)^{2.3} \times (5 - 20\omega)^{3.3} (5.5 + |10^5 \eta|)^{2.4} e^{-11.8} - 1 \quad (3)$$

where $\frac{\partial u}{\partial x}$ is the meridional gradient of zonal wind at 500 hPa; ω is the 500 hPa vertical pressure velocity. The DGPI was derived from both the present day and future global warming environment. It works better than ENGPI on inter-annual time-scale and under high emission forced global warming climate (Wang and Murakami 2020, Murakami and Wang 2022). Both GPIs represent the observed present-day TC climatology very well (Wang and Murakami 2020, Cao *et al* 2021), and the ensemble mean of historical simulation can well reproduce the observed TCF climatology for NH during JASO and SH during JFMA (Cao *et al* 2021). The observed NH TC frequency shows an increasing trend and the SH TC frequency shows an decreasing trend since the 1980s when the available TC frequency data is reliable. The trends may partially attribute to the external forcings (Murakami *et al* 2020). The multi-model ensemble means of ENGPI and DGPI well simulated the increase and decrease trend over the NH and SH, respectively (figure S1). It suggests the robustness of the usage of the two GPIs during the historical period and the reliability of the 14 CMIP6 model simulations.

3. Main results

3.1. Changes in GPIs response to external forcing

Figure 1 shows the impacts of historical ALL, aerosol, and GHG forcing during TC peak season from the ENGPI and DGPI based upon the ensemble mean of 14 CMIP6 models. Overall, the ENGPI and



DGPI show a similar spatial pattern of anomalies for the giving forcing (e.g. aerosol, GHG, and their combined), indicating the response pattern is robust regardless of the type of GPI (ENGPI and DGPI; figure 1). When considering aerosol and GHG forcing simultaneously (figures 1(a) and (b)), the anomalies of GPIs are apparently smaller than that from any individual forcing (figures 1(c)–(f)). It confirms our hypothesis that the comparable and opposite impacts of the two forcings exist on global TCF. The simulated GPI anomalies in the historical experiment generally increases over the SH, while it is basin-dependent over the NH for ENGPI and DGPI. Specifically, there is a triple response pattern over the Northwestern Pacific (WNP), a dipole pattern over the Northeastern Pacific, and a uniform decreased pattern over the North Atlantic. The reduction of TCF over the North Atlantic is consistent with the observed long-term change. Some studies compiled the long-term TC frequency datasets over the North Atlantic based on ship reports, journals, and marine proxy data (Nybery *et al* 2007, Vecchi and Knutson 2011, Vecchi *et al* 2021). The compiled North Atlantic TC datasets show more TCs during the pre-industrial period than in the present-day climate.

In terms of individual forcing, the hist-aer experiment simulated an apparent decrease of GPIs over the NH oceans (figure 1(c)), while over the SH there is an overall increase and southward shift of GPIs (figure 1(d)). It agrees well with the results from the ensemble simulations of climate models with

comprehensive aerosol effects and CMIP5/CMIP6 simulation with different complexity treatments of aerosol (Dunstone *et al* 2013, Cao *et al* 2021, Murakami 2022). The GHG-induced changes of GPIs are generally similar to that in hist-aer run, but the sign is reversed (figures 1(c)–(f)). The simulated GPIs are increased over most part of the North Pacific, the main development zone of the North Atlantic, but decreased over the southeast part of WNP, western coast of North America, Gulf of Mexico, and the Caribbean Sea (figures 1(e) and (f)). This pattern coincides with the results from high-resolution models as suggested by previous studies (Zhao *et al* 2009, Li *et al* 2010, Roberts *et al* 2015, Bhatia *et al* 2018, Knutson *et al* 2020), while some studies show opposite results (Sugi and Yoshimura 2012, Knutson *et al* 2013, Murakami *et al* 2014, Satoh *et al* 2015). It suggests the high uncertainty of the projected TCF changes over individual basins, although the majority of studies suggested that GHG-induced global warming could reduce the global TCs (Sugi and Yoshimura 2012, Satoh *et al* 2015, Knutson *et al* 2020).

The competing effect from GHG and aerosol forcing largely dominates the relative weak change of GPIs under historical ALL forcing (figure 1). This is further confirmed by the high consistency of spatial pattern between historical simulation and the sum of GPI changes from hist-GHG and his-aer runs in both ENGPI and DGPI (figure S2). It suggests that the GPI responses to GHG and aerosol forcing are probably linearly additive during the historical period. The

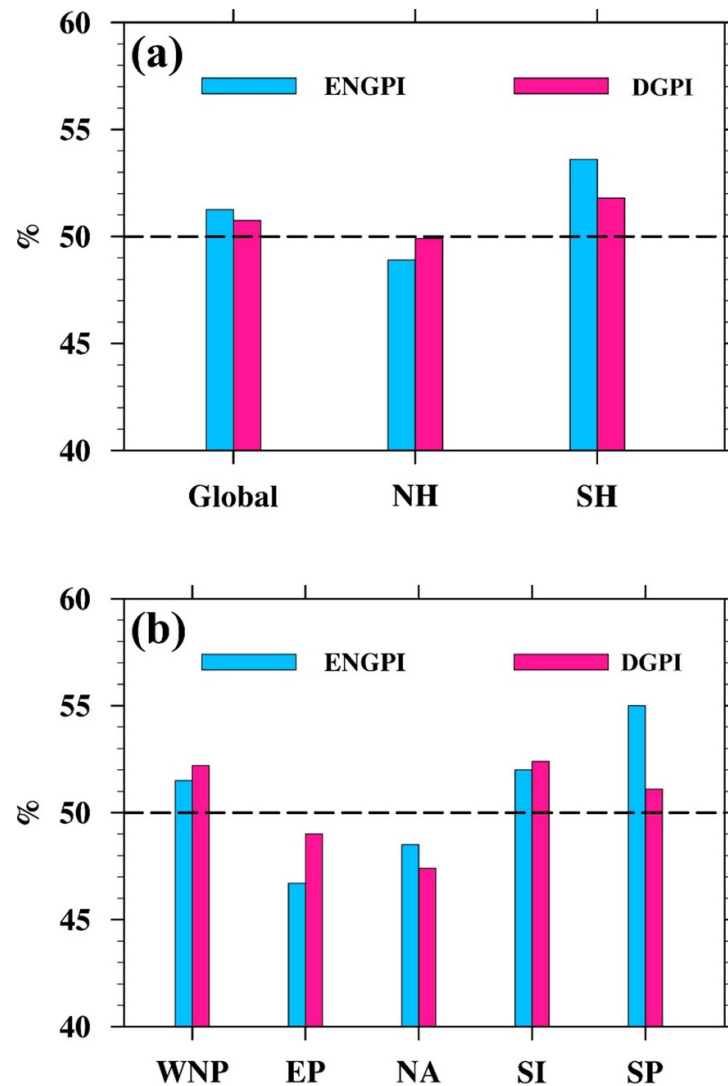


Figure 2. The contributions of aerosol forcing in changing ENGPI and DGPI for (a) global and (b) individual ocean basins.

result agrees well with the impacts of these two forcings on PI as suggested by Ting *et al* (2015) and Sobel *et al* (2016). It raises our confidence to untangle the relative importance of individual external forcing based upon the single forcing experiments from CMIP6 models.

3.2. Comparable impacts of aerosol and GHG forcing on GPIs

To quantitatively assess the relative importance of the forcing (factor) on GPI anomalies, we defined the importance index for a giving forcing (factor) as:

$$Con_f1 = \frac{|eff_f1|}{|eff_f1| + |eff_f2|} \quad (4)$$

where $f1$ and $f2$ can be either aerosol or GHG forcing. $|eff_f1|$ and $|eff_f2|$ are the magnitudes of GPI anomalies to the individual forcing, respectively. By definition, the Con_f2 is equal to $1-Con_f1$. Figure 2 explicitly shows the relative importance of the aerosol

forcing for the GPI anomalies over the global, hemispheric, and individual ocean basins. The contributions from the aerosol forcing are ~51%, 49%, and 54% for the global, NH, and SH GPI anomalies in ENGPI, respectively. Similarly, the contributions are ~51%, 50%, and 52% from DGPI, respectively (figure 2(a)). Regionally, contributions range from 45% to 55% over individual ocean basins in both GPIs (figure 2(b)). The two TCF proxies consistently show a relatively larger effect from aerosol forcing over the WNP, South Indian Ocean, and South Pacific Ocean, but a smaller impact over the eastern Pacific and the North Atlantic. These results suggest the comparable importance of aerosol and GHG forcing for GPI anomalies over the global and hemisphere scales, although the regional feature exists. Therefore, the plausible speculation no detectable impact from human activities on global TCF during the recent decades could be due to the cancellation of the obvious impacts from individual anthropogenic forcing.

To reveal the key factors that dominate the GPI changes and identify why the GPI changes are comparable between the two forcings, we decomposed the ENGPI (DGPI) in figure S3 (figure S4) following previous studies (Camargo *et al* 2007, Zhao *et al* 2018, Cao *et al* 2021). The decomposition is designed by replacing one variable with its present-day (pd) (1985–2014) value but fixing the rest at their pre-industrial (pi) values. For instance, the GPI anomaly for a giving variable is defined as:

$$\begin{aligned}\Delta\text{GPI}_{\text{var1}} &= \text{GPI}_{\text{var1}} - \text{GPI}_{\text{pi}} \\ &= (\text{Var1}_{\text{pd}} - \text{Var1}_{\text{pi}}) * \text{Var2}_{\text{pi}} * \text{Var3}_{\text{pi}} * \text{Var4}_{\text{pi}}\end{aligned}\quad (5)$$

Following it, the GPI anomalies from each factor (e.g. $\Delta\text{GPI}_{\text{var2}}$, $\Delta\text{GPI}_{\text{var3}}$, $\Delta\text{GPI}_{\text{var4}}$) can be calculated. Figure S5 compared the sum of the four factors-induced GPI anomalies and the GPI anomaly from the aerosol and GHG forcing. It shows that this decomposition is well linearly additive for both GPIs under aerosol and GHG forcing.

Figures S3 and S4 illustrate the impact of individual factors from ENGPI and DGPI. The results show that the effects from PI and VWS dominate the changes of ENGPI in hist-GHG and hist-aer experiments (figure S3). In the hist-aer experiment, the PI has a negative effect on ENGPI, especially over the NH TC development zone (figure S3(a)). The contribution of VWS has significant regional features with a generally positive impact over the SH but a negative effect over the NH, except for the southwest part of WNP (figure S3(c)). This pattern resembles the NH-decreased and SH-increased TCF changes under aerosol forcing (figure 1(c)), suggesting that the VWS plays a vital role in shaping the TC formation pattern. When forced by GHG, the impacts from PI and VWS generally show similar patterns to that of the aerosol forcing, except for the sign (figures S3(b) and (d)). The contributions of RH and VORT are both small compared to PI and VWS in the two experiments (figures S3(f) and (h)).

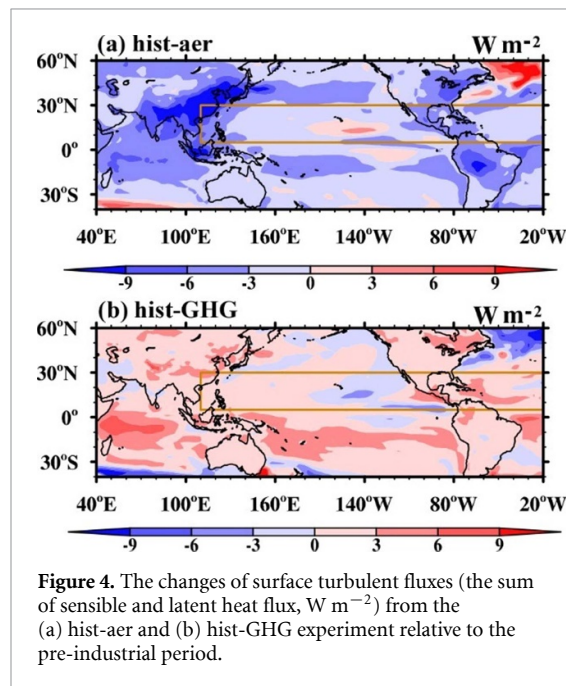
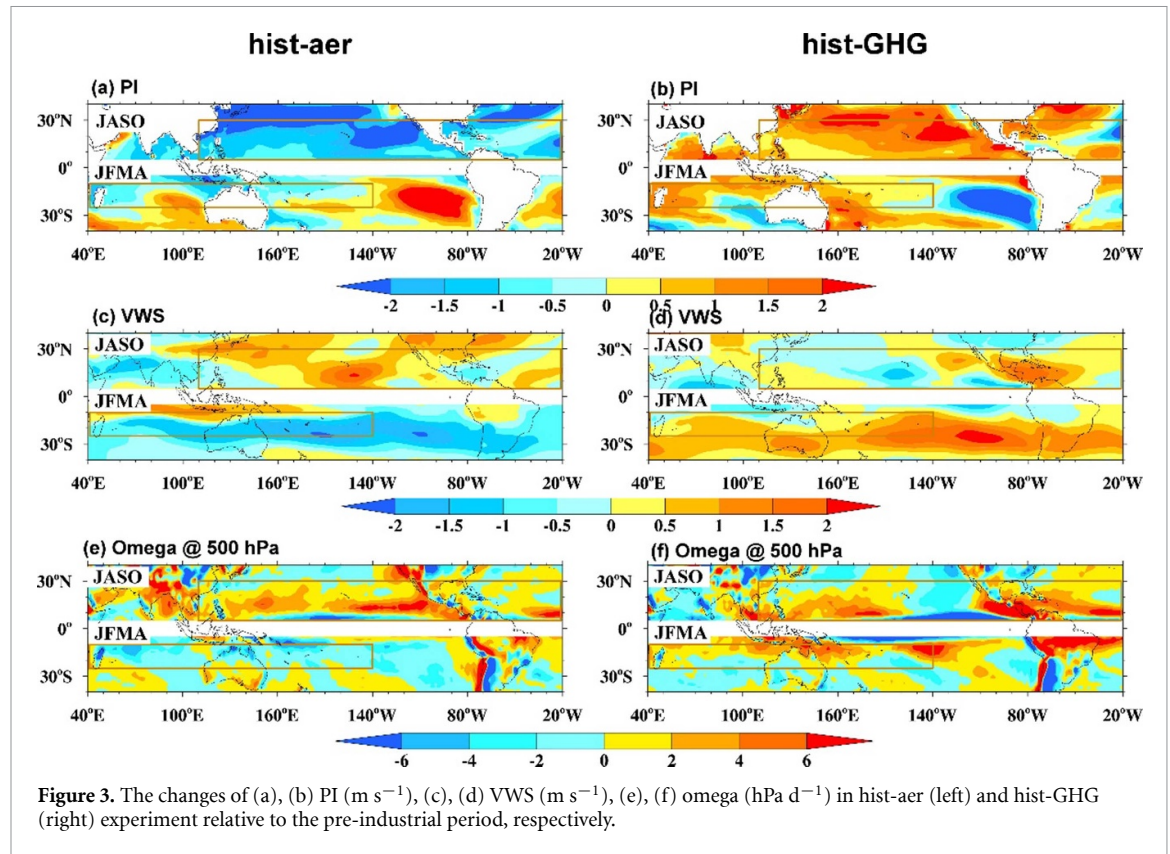
The decompositions of DGPI show that the impacts of VWS and Omega are the major contributors to DGPI changes under both aerosol and GHG forcing (figure S4). The effect of VWS (Omega) shares a similar spatial pattern but in different signs between the two forcings. In addition, figure S6 quantitatively compared the impacts from PI, VWS, and Omega in changing GPIs between the two forcings over the global and regional scales using equation (4). It shows that the impacts of a giving factor (e.g. PI, VWS, and Omega) on GPIs are generally comparable between aerosol and GHG forcing over the hemispheric scale and ocean basin scale. That means the dominant contributors to the GPI anomalies are comparable between the historical aerosol and GHG forcing.

3.3. Comparable impacts on TC environment from aerosol and GHG forcing

Why are the TC environment impacts on GPIs comparable between the aerosol and GHG forcing? Figure 3 shows the changes of PI, VWS, and Omega under the two forcings. The PI anomaly shows a significant increase over the NH and a slight increase over the SH TC development zones under GHG forcing, while the aerosols could induce a similar pattern of PI reduction, especially over the NH (figures 3(a) and (b)). It means that the aerosol cooling could cancel out the GHG warming-induced PI increase, indicating the approximately equal influences on TC potential intensity in the CMIP6 models (figures 3(a) and (b)). Therefore, the comparable impact of PI-induced GPI changes is attributable to the comparable PI changes between the two forcings (figure 3). Sobel *et al* (2019) suggested that the net surface turbulent heat flux (sum of sensible and latent heat flux) plays a dominant role in explaining the PI differences between aerosol and GHG forcing. Figure 4 illustrates the negative net surface turbulent heat flux from the hist-aer and the positive heat flux from hist-GHG experiment. Indeed, they are in a comparable magnitude over the NH TC development zone. The high consistency between the CMIP5 model result and our analyses confirms the cancelation effect between the two forcings on the TC environment (Sobel *et al* 2016, 2019, Ting *et al* 2015).

The hist-aer experiment simulated enhanced VWS over most NH oceans but weakened it over the SH TC development zone (figure 3(c)). The change in VWS under GHG forcing remarkably resembles that under aerosol forcing, except for the sign (figures 3(c) and (d)). The difference in the sign of VWS changes between the two forcings is attributable to the two factors. First, the opposite responses of both the lower and upper tropospheric circulation are seen over the NH TC development zone (figure S7). Second, over the SH, the upper-level subtropical westerly jet weakened and strengthened, respectively, under the aerosol and GHG forcing (figures S8(c) and (d)), and the responses of the low-level circulation are relatively small (figures S8(a) and (b)).

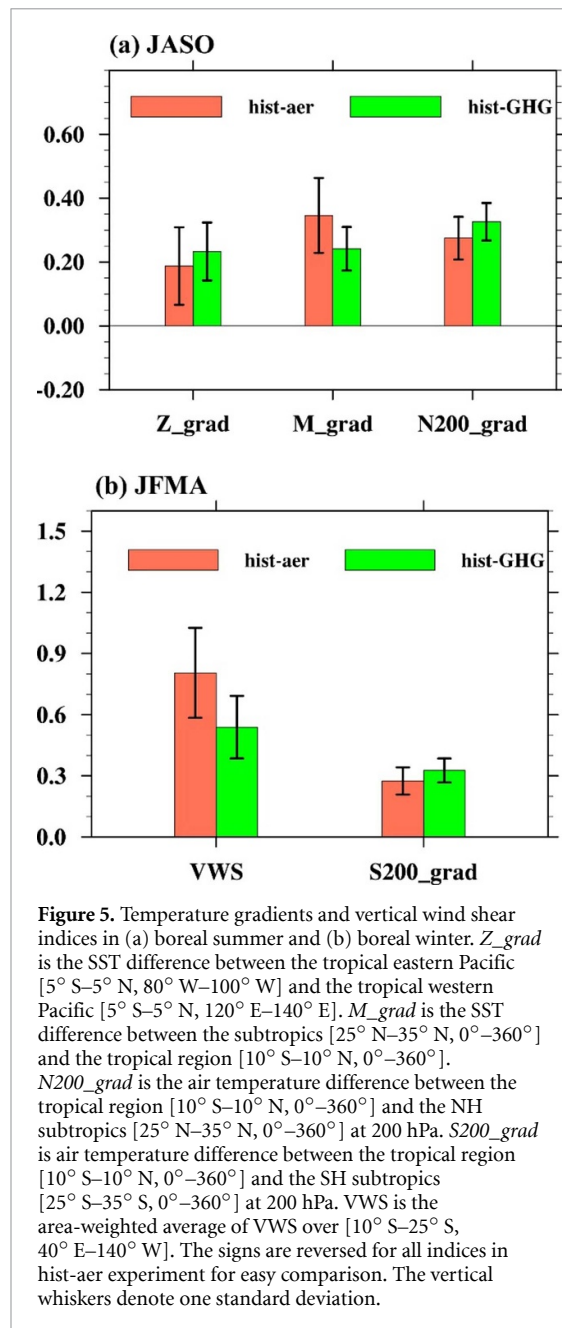
The changes of temperature gradients are responsible for the circulation changes under both forcings. To quantitative compare the temperature gradients, the indices are defined as follows: the zonal gradient of SST over the tropical pacific ocean (Z_grad) is calculated as the SST difference between the tropical eastern Pacific [5°S – 5°N , 80°W – 100°W] and the tropical western Pacific [5°S – 5°N , 120°E – 140°E], the meridional SST gradient over NH (M_grad) is defined as the SST difference between subtropics [25°N – 35°N , 0° – 360°] and tropical region [10°S – 10°N , 0° – 360°], and the meridional gradient of upper-troposphere temperature over the NH ($N200_grad$) is defined as the air temperature difference between tropical



region [10°S – 10°N , 0° – 360°] and the NH subtropics [25°N – 35°N , 0° – 360°] at 200 hPa, and the meridional gradient of upper-troposphere temperature over the SH ($S200_grad$) is the difference between the tropical region [10°S – 10°N , 0° – 360°] and the SH subtropics [25°S – 35°S , 0° – 360°] at 200 hPa.

During the JASO season, the opposite and similar magnitude of zonal and meridional SST gradients across the Northern tropical Pacific Ocean (Z_grad , M_grad) drive the opposite changes in low-troposphere circulation from the aerosol and GHG forcing (figure 5(a)). The change in the upper troposphere circulation is in a similar magnitude but with different signs. It is attributable to the similar magnitudes of tropical to subtropical upper-troposphere temperature gradients ($N200_grad$) at 200 hPa in hist-aer and hist-GHG experiments (figure 5(a)), although the physical mechanism is different. The enhancement of the upper-troposphere temperature gradient is due to the top-heavy heating over the tropics in the hist-GHG experiment, while it is due to the reduction of temperature gradient caused by the NH preferring cooling in the hist-aer experiment (figures S9(a) and (c)). During the JFMA season, the opposite-in-sign changes of VWS are dominated by the upper-level subtropical jet over the SH (figures S7(c) and (d)). It can be explained by the thermal wind balance due to the opposite changes of upper-troposphere temperature gradients ($S200_grad$) between the two forcings (figures 5(b) and S9(b), (d)). Thus, the opposite signs of VWS change between the two forcings are attributable to the opposite atmospheric-ocean temperature gradients (figure 5).

The response of mid-troposphere vertical motion in the hist-GHG experiment is generally opposite to



that of in hist-aer experiment over the SH in austral summer, but both aerosol and GHG forcing generally weaken the NH ascent motion in boreal summer (figures 3(e) and (f)). The changes in vertical motion are well consistent with the zonal mean Hadley circulation changes (figure S10), although the driving mechanisms are different between the two forcings. The anthropogenic aerosol forcing prefers to cool the NH than the SH (figures S7(a) and S8(a)), thereby decreasing/increasing the interhemispheric temperature difference in the boreal/austral summer, thus weakening/strengthening the climatologic ascending motion over the NH/SH (figures 3(e) and (f)). However, the increase of GHG forcing produces the top-heavy heat of the atmosphere over the tropics (figures S9(c) and (d)), which enhances the atmospheric stability over both hemispheres, leading to the

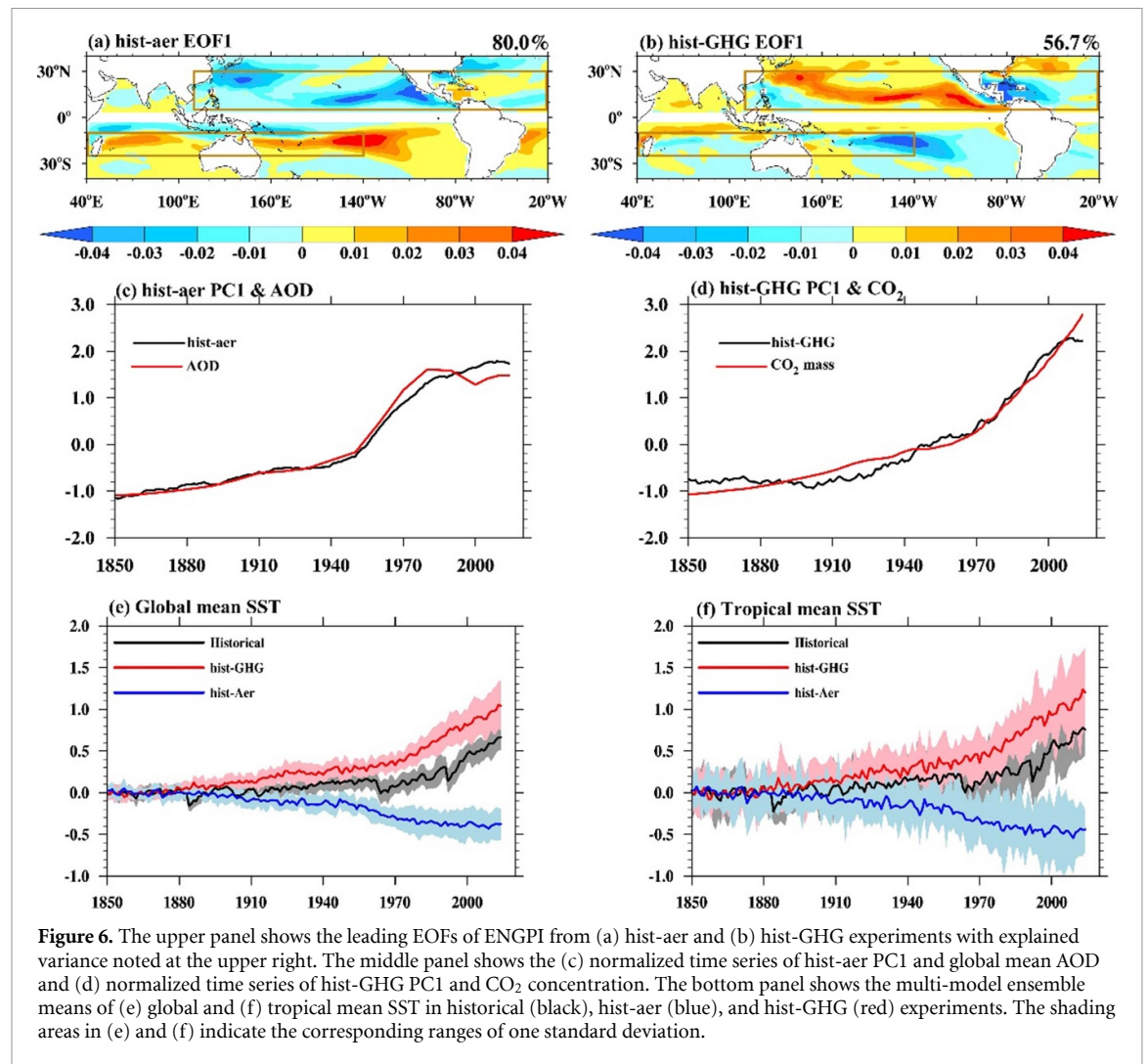
weakened vertical motion over the tropics. In addition, the significant zonal variation of vertical motion exists in the hist-GHG experiment, and it may be caused by the El-Nino type of SST warming over the Pacific Ocean.

In sum, the TC-related environment shows similar responses to both the aerosol and GHG forcing, leading to the comparable impact of the individual factor on the GPI change between the two forcings. Since the effects of the two forcings are in different signs on GPI, they could cancel out each other during the historical period when the two forcings are coexistence. It may result in insignificant changes of the TC-related environment, thus the global TC frequency.

3.4. Persistent cancellation effect during the historical period

During the historical period, the anthropogenic aerosol and GHG forcing are both continually increased, thus competition always exists due to the similar temporal evolution of the two forcings (figures 6(c) and (d)). We apply the empirical orthogonal function (EOF) analysis to the ENGPIs in his-aer and hist-GHG experiments during 1850–2014. The EOF1s from hist-aer and hist-GHG experiments are similar to the corresponding GPI anomalies between the present-day (1985–2014) and pre-Industrial period (figures 1(a) and (b)), showing the cancellation pattern between the two forcings (figures 6(a) and (b)). On the temporal evolution, the principal component for aerosol-induced response shows a slow increase before the 1950s, an upward rapidly for 1950s–1990s followed by stalls. Its temporal evolution well agrees with the global mean aerosol optical depth and global/tropical mean SST (figures 6(c), (e) and (f)). Forced by the observed GHG emission, the simulated first principal component of ENGPI features weak variation before the 1940s, a weak upward for the 1950s–1970s, and a robust rising trend after the 1970s (figure 6(d)). Therefore, the two principal components have roughly a similar pace of changes; thus, the competition between the two leading modes could lead to a weaker change in GPI during the historical period.

As calculated in table 1, the effective radiative forcing from anthropogenic aerosol is about -1.14 W m^{-2} ; it is about one-third of that from GHG forcing ($+2.94 \text{ W m}^{-2}$). Correspondingly, the aerosol cooling effect is about half of the GHG warming effect on global (-0.38 vs 0.80 K) and tropical (-0.45 vs 0.94 K) SST (e.g. 1985–2014 minus piControl climatology, figures 6(e) and (f)). However, the changes in TC-related environment are almost comparable in the two forcings (figure 5), implying that the aerosol-induced global cooling more effectively modulates atmospheric circulation, by about a factor of two for a unit SST change, than the GHG-induced global warming. Therefore, the TCs are more sensitive



to the aerosol forcing than the GHG forcing in terms of global radiative forcing and global (tropical) mean SST.

4. Conclusion

The historical and single anthropogenic forcing experiments from 14 CMIP6 models are used to understand the climate impacts of anthropogenic aerosol and GHG forcing on global TCF. Two GPIs, thermodynamic–dynamic-based ENGPI and pure dynamic-orient DGPI, are both used as TC frequency proxies. The responses are consistent for the two TCF proxies under various forcings during the historical period, verifying the robustness of our result. It shows that the historical aerosol loading and GHG emission can significantly alter global TCs, while global TCF response is relatively small in the historical experiment. We quantified the relative importance of the aerosol and GHG forcing in changing global TCF by decomposing both the ENGPI and DGPI. Our results indicate that the changes in TCF associated with aerosol and GHG forcing are almost comparable but opposite. It is mainly due to the similar

atmospheric-ocean thermal gradients under the two forcings, which cause the same magnitude changes of the TC-environmental conditions (e.g. PI, VWS, and Omega) under the aerosol and GHG forcing, regardless of their opposite signs. The radiative forcing from anthropogenic aerosol is about one-third of that of GHG forcing. The global (tropical) SST change induced by the aerosol forcing is about half of that induced by GHG forcing. These facts together imply that the aerosol forcing has a higher efficiency in causing TCF changes for a unit of radiative forcing and tropical mean SST change. The higher efficiency is due to the aerosol forcing being more effective in changing atmospheric-ocean temperature gradients.

Our results proposed a possible explanation for the important scientific issue: why the global TCF has been relatively stable over the past decades under the background of intensive anthropogenic influence. There could be an insignificant trend of TCF when combining the two anthropogenic forcings since their impacts are primarily canceled by each other. When considering the forcing separately, the impact of individual anthropogenic forcing on hemispherical/regional TCF may be detectable. As shown by this

study, global TCF is both substantially affected by aerosol and GHG forcing, future changes in global and regional TCs and their associated impacts, therefore, are dependent on the aerosol and GHG emission policies.

Data availability statement


The data that support the findings of this study are openly available at the following URL/DOI: <https://esgf-node.llnl.gov/search/cmip6/>.

Acknowledgments

Jian Cao acknowledges the support from the Natural Science Foundation of China of Jiangsu Province (BK20220108) and Natural Science Foundation of China (41730961, 42005017). Haikun Zhao acknowledges the support from the Natural Science Foundation of China (41922033). We acknowledge the computer resources at the NUIST High Performance Computer Center. This is ESMC publication NO.383 and IPRC publication NO.1575.

ORCID iDs

Jian Cao  <https://orcid.org/0000-0001-9105-9400>

Haikun Zhao  <https://orcid.org/0000-0002-1771-1461>

References

- Bhatia K, Vecchi G, Murakami H, Underwood S and Kossin J 2018 Projected response of tropical cyclone intensity and intensification in a global climate model *J. Clim.* **31** 8281–303
- Camargo S 2013 Global and regional aspects of tropical cyclone activity in the CMIP5 models *J. Clim.* **26** 9880–902
- Camargo S, Emanuel K and Sobel A 2007 Use of a genesis potential index to diagnose ENSO effects on tropical cyclone genesis *J. Clim.* **20** 4819–34
- Cao J, Zhao H, Wang B and Wu L 2021 Hemisphere-asymmetric tropical cyclones response to anthropogenic aerosol forcing *Nat. Commun.* **12** 6787
- Dunstone N, Smith D M, Booth B B B, Hermanson L and Eade R 2013 Anthropogenic aerosol forcing of Atlantic tropical storms *Nat. Geosci.* **6** 534–9
- Emanuel K 2021 Response of global tropical cyclone activity to increasing CO₂: results from downscaling CMIP6 models *J. Clim.* **34** 57–70
- Emanuel K and Nolan D 2004 Tropical cyclone activity and global climate *Bull. Am. Meteorol. Soc.* **85** 240–1
- Eyring V, Bony S, Meehl G A, Senior C A, Stevens B, Stouffer R J and Taylor K E 2016 Overview of the coupled model intercomparison project phase 6 (CMIP6) experimental design and organization *Geosci. Model Dev.* **9** 1937–58
- Gillett N P, Shioyama H, Funke B, Hegerl G, Knutti R, Matthes K, Santer B D, Stone D and Tebaldi C 2016 The detection and attribution model intercomparison project (DAMIP v1.0) contribution to CMIP6 *Geosci. Model Dev.* **9** 3685–97
- Jones A C, Haywood J M, Dunstone N, Emanuel K, Hawcroft M K, Hodges K I and Jones A 2017 Impacts of hemispheric solar geoengineering on tropical cyclone frequency *Nat. Commun.* **8** 1382
- Knutson T R et al 2019 Tropical cyclones and climate change assessment: part I. Detection and attribution *Bull. Am. Meteorol. Soc.* **100** 1987–2007
- Knutson T R et al 2020 Tropical cyclones and climate change assessment: part II. Projected response to anthropogenic warming *Bull. Am. Meteorol. Soc.* **101** 303–22
- Knutson T R, McBride J L, Chan J, Emanuel K, Holland G, Landsea C, Held I, Kossin J P, Srivastava A K and Sugi M 2010 Tropical cyclones and climate change *Nat. Geosci.* **3** 157–63
- Knutson T R, Sirutis J J, Vecchi G A, Garner S, Zhao M, Kim H, Bender M, Tuleya R E, Held I M and Villarini G 2013 Dynamical downscaling projections of twenty-first-century atlantic hurricane activity: CMIP3 and CMIP5 model-based scenarios *J. Clim.* **26** 6591–617
- Lee C, Camargo S and Sobel A 2020 Statistical–dynamical downscaling projections of tropical cyclone activity in a warming climate: two diverging genesis scenarios *J. Clim.* **33** 3515–4834
- Li T, Kwon M, Zhao M, Kug J, Luo J and Yu W 2010 Global warming shifts Pacific tropical cyclone location *Geophys. Res. Lett.* **37** L21804
- Murakami H 2022 Substantial global influence of anthropogenic aerosols on tropical cyclones over the past 40 years *Sci. Adv.* **8**
- Murakami H, Delworth T L, Cooke W F, Zhao M, Xiang B and Hsu P 2020 Detected climatic change in global distribution of tropical cyclones *Proc. Natl. Acad. Sci.* **117** 10706–14
- Murakami H, Hsu P-C, Arakawa O and Li T 2014 Influence of model biases on projected future changes in tropical cyclone frequency of occurrence *J. Clim.* **27** 2159–81
- Murakami H and Wang B 2022 Patterns and frequency of projected future tropical cyclone genesis are governed by dynamic effects *Commun. Earth Environ. Sci.* **3** 77
- Nyberg J, Malmgren B A, Winter A, Jury M R, Kilbourne K H and Quinn T M 2007 Low Atlantic hurricane activity in the 1970s and 1980s compared to the past 270 years *Nature* **447** 698–701
- O'Neill B C et al 2016 The scenario model intercomparison project (ScenarioMIP) for CMIP6 *Geosci. Model Dev.* **9** 3461–82
- Pausata F S and Camargo S J 2019 Tropical cyclone activity affected by volcanically induced ITCZ shifts *Proc. Natl. Acad. Sci.* **116** 7732–37
- Persad G G, Ming Y, Shen Z and Ramaswamy V 2018 Spatially similar surface energy flux perturbations due to greenhouse gases and aerosols *Nat. Commun.* **9** 1–7
- Roberts M J, Vidale P Luigi, Mizielinski M S, Demory M, Schiemann R, Strachan J, Hodges K, Bell R and Camp J 2015 Tropical cyclones in the upscale ensemble of high-resolution global climate models* *J. Clim.* **28** 574–96
- Satoh M, Yamada Y, SUGI M, Kodama C and Noda A T 2015 Constraint on future change in global frequency of tropical cyclones due to global warming *J. Meteorol. Soc. Japan* **93** 489–500
- Sobel A H, Camargo S J, Hall T M, Lee C-Y, Tippett M K and Wing A A 2016 Human influence on tropical cyclone intensity *Science* **353** 242–6
- Sobel A H, Camargo S J and Pervidi M 2019 Aerosol versus greenhouse gas effects on tropical cyclone potential intensity and the hydrologic cycle *J. Clim.* **32** 5511–27
- Sugi M and Yoshimura J 2012 Decreasing trend of tropical cyclone frequency in 228-year high-resolution AGCM simulations *Geophys. Res. Lett.* **39** L19805
- Taylor K E, Stouffer R J and Meehl G A 2012 An overview of CMIP5 and the experiment design *Bull. Am. Meteorol. Soc.* **93** 485–98
- Ting M, Camargo S J, Li C and Kushnir Y 2015 Natural and forced North Atlantic hurricane potential intensity change in CMIP5 models *J. Clim.* **28** 3926–42
- Vecchi G A and Knutson T R 2011 Estimating annual numbers of Atlantic hurricanes missing from the hurdat database

- (1878–1965) using ship track density *J. Clim.* **24** 1736–46
- Vecchi G A, Landsea C, Zhang W, Villarini G and Knutson T 2021 Changes in Atlantic major hurricane frequency since the late-19th century *Nat Commun* **12** 4054
- Villarini G and Vecchi G A 2013 Twenty-first-century projections of North Atlantic tropical storms from CMIP5 models *Nat. Clim. Change* **2** 604–7
- Walsh K J E et al 2016 Tropical cyclones and climate change *Wiley Interdiscip. Rev.* **7** 65–89
- Wang B and Murakami H 2020 Dynamic genesis potential index for diagnosing present-day and future global tropical cyclone genesis *Environ. Res. Lett.* **15** 114008
- Wang Q, Moore J and Ji D 2018 A statistical examination of the effects of stratospheric sulfate geoengineering on tropical storm genesis *Atmos. Chem. Phys.* **18** 9173–88
- Webster P J, Holland G J, Curry J A and Chang H-R 2005 Changes in tropical cyclone number, duration, and intensity in a warming environment *Science* **309** 1844–6
- Weinkle J, Maue R and Pielke R 2012 Historical global tropical cyclone landfalls *J. Clim.* **25** 4729–35
- Xie S P, Lu B and Xiang B 2013 Similar spatial patterns of climate responses to aerosol and greenhouse gas changes *Nat. Geosci.* **6** 828–32
- Zhao H, Chen S, Klotzbach P J and Raga G B 2018 Impact of the extended boreal summer intra-seasonal oscillation on western north Pacific tropical cloud cluster genesis productivity *J. Clim.* **31** 9175–91
- Zhao M, Held I M, Lin S and Vecchi G A 2009 Simulations of global hurricane climatology, interannual variability, and response to global warming using a 50-km resolution GCM *J. Clim.* **22** 6653–78